JOURNAL OF MATERIALS SCIENCE **34** (2000) 925–929

Tensile mechanical behavior of TiAl(FL) at high strain rate

YUANXIN ZHOU, YUANMING XIA
Department of Modern Mechanics, University of Science and Technology of China, Hefei, Anhui 230027
E-mail: ymxia@ustc.edu.cn

The tensile mechanical behavior of Ti-47at%Al-1.5at%Cr-0.5ar%Mn-2.8at%Nb in full lamellar microstructure has been studied in the strain rate range from 100 s^{-1} to 800 s^{-1} and the complete stress-strain curves were obtained. Results show that the alloy is extremely brittle at different strain rate, exhibiting near-zero ductility. Both UTS and fracture strain of material are strain rate sensitive, increasing with the strain rate at room temperature. Fractography analysis indicates that the alloy fractures in a mixed mode of predominant transgranular cleavage and minor intergranular cracking. On basis of the experiment results and Weibull distribution theory, a statistic model has been developed to describe mechanical behavior of TiAl(FL) at different strain rate. The statistical parameters for material and their relationships with strain rate are obtained from tensile impact experimental results. The simulated stress strain curves from the model are in good agreement with the test data. The theoretical model and test results show that both the scale parameter σ_0 and the shape parameter β are rate dependent, and a linear dependence of σ_0 and β on $\lg \dot{\varepsilon}$ has been found.

1. Introduction

Gamma TiAl have attracted a great deal of attention from the aerospace community during the last 20 years, and also from the automobile industry, because of their potentially attractive properties for high temperature structural applications such as low density, good oxidation and burn resistance, and high-temperature strength retention [1–3]. Thanks to the extensive research and development activities in alloy development seen during this period, there are now several gamma TiAl alloys of engineering importance based on Ti-(46-48)Al. Room temperature mechanical properties of these alloy are known to strongly depend on microstructure. The variations of microstructure that can be controlled in these alloy are numerous, but they exist in four broad groupings; that is near-gamma (NG), duplex (DP), nearly-lamellar (NL) and fully-lamellar (FL) microstructure [4]. A number of mechanical property measurements have been made on these microstructures [5–7]. Results show that FL microstructure exhibit poor ductility and lower RT strength in general, but room-temperature fracture toughness values of it is higher than that of other three microstructure [8].

At present, the mechanical behavior of TiAl alloy have usually characterized in items of quasi-static loading, although some structural applications require good performance during impact or high rate deformation. Only a limited amount of research has been concerned with the mechanical response of TiAl alloy at high strain rate. Maloy [9] has studied the mechanical behavior and resulting deformation substructure of a Ti-48-1V alloy at high strain rate by SHPB at different temperature. A rate sensitivity of 0.029 was observed for deformation at room temperature. Follansbee and Gray [10] also studied the high strain rate response of the TiAl alloy between 77 K to 495 K. However, these deformation modes are all limited to compression. Tensile properties of TiAl alloy at high strain rate, which are surely more typical than compressive properties, are not to be investigate yet.

In the present paper, using our own design of bar-bar tensile impact apparatus with a high speed rotating disk, the tensile test of Ti-47at%Al-1.5at%Cr-0.5ar%Mn-2.8at%Nb in full lamellar microstructural under tensile impact in the strain rate range from 100 s^{-1} to 800 s^{-1} were carried out and the complete stress-strain curves of material under tensile impact were obtained. Based on the experimental results, we reveal the dynamic behavior of TiAl alloy and have derived a one-dimensional macro constitutive equation describing the composite under tensile impact by using the Weibull distribution theory.

2. Tensile impact experiment

2.1. Experimental apparatus and principle

The self-designed rotating disk tensile impact bar-bar apparatus [11] and its measuring principle are shown in Fig. 1. As the hammer on the high-speed rotating disk impacts the block, the short metal bar (made of aluminum alloy) breaks and an approximately rectangular input stress impulse is produced and transmitted

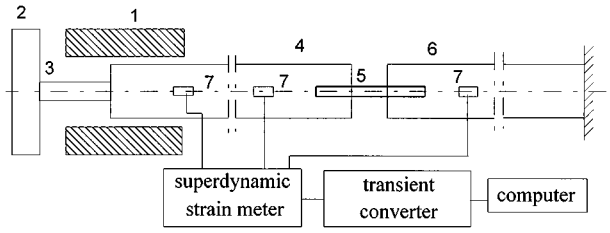

Figure 1 Schematic diagram of tensile impact set-up and principle of measurement 1—hammer, 2—block, 3—short metal bar, 4—input bar, 5—specimen, 6—output bar, 7—strain gauges.

through the input bar to the specimen. The partial impulse is reflected to the input bar and survival impulse is transferred to the output bar. Comparing with other tensile impact bar-bar apparatus, the principle of impulse producing in our apparatus is brand-new. Tensile impulse is not produced by the impacting the block with the hammer directly, but by elastic-plastic deformation to fracture of short metal bar. Adjusting the speed and diameter or length of short metal bar, the amplitude, width and rising gradient with the different tensile impulse can be obtained. By applying different amplitude stress impulse, tensile impact tests at different strain rate of different materials can be carried out. If short stress impulse are used, tensile impact loading-unloading tests at different strain rate of different materials can be achieved.

The wave signals are recorded on a transient converter through a super dynamic strain meter. The formula of strain $\varepsilon_s(t)$, strain rate $\dot{\varepsilon}_s(t)$, and stress $\sigma_s(t)$ of the specimens are as follows:

$$\varepsilon_s(t) = \frac{c_0}{L_0}\int_0^t [\varepsilon_i(\tau) - \varepsilon_r(\tau) - \varepsilon_t(\tau)]\,d\tau \quad (2.1)$$

$$\dot{\varepsilon}_s(t) = \frac{c_0}{L_0}[\varepsilon_i(t) - \varepsilon_r(t) - \varepsilon_t(t)] \quad (2.2)$$

$$\sigma_s(t) = \frac{EA}{2A_0}[\varepsilon_i(t) + \varepsilon_r(t) - \varepsilon_t(t)] \quad (2.3)$$

where E, A and C_0 are the modulus, cross-section and elastic wave speed of input bar and output bar respectively, and L_0 and A_0 are the length and cross-section of the testing part of the specimen. Input stress wave $\varepsilon_i(t)$ and reflective stress wave $\varepsilon_r(t)$ can be measured by strain gauges on the input bar, and the transmission wave $\varepsilon_t(t)$ can be measured by strain gauges on the output bar also.

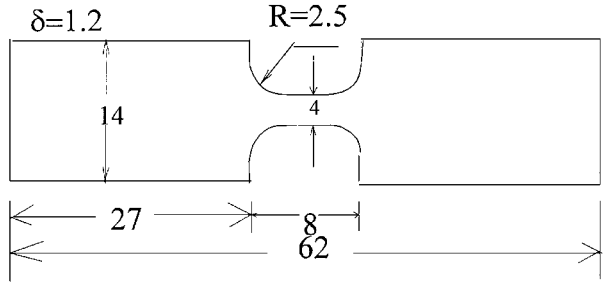

(a)

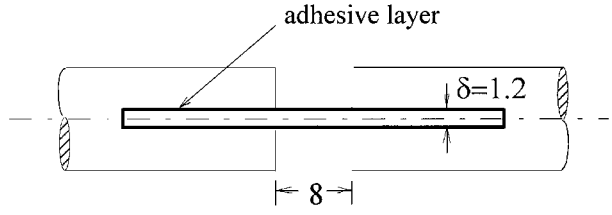

(b)

Figure 2 (a) Configuration of specimen; (b) configuration of specimen.

2.2. Specimen and its connection

Ingots of Ti-47at%Al-1.5at%Cr-0.5ar%Mn-2.8at%Nb were prepared by skull melting/castion. The casting ingots were annealed for homogenization and then isothermally forged into plates. Then, the plates were heat-treated at 1567 K for 3 hours and furnace cooled to 1173 K, further air cooled to room temperature. Finally, the plates were annealed at 1658 K for 20 minutes and FL microstructure were obtained. The specimen were cut from plates by electro-discharging machining (Fig. 2a), and the specimen is connected to input-bar and output-bat by AS-103 adhesive (Fig. 2b).

2.3. Tensile impact tests

By controlling the height and the range of input pulse, three groups (corresponding to strain-rate of 100 s^{-1}, 300 s^{-1} and 800 s^{-1}) of tensile impact test for TiAl have been performed. The typical experimental wave under tensile loading is shown in Fig. 3.

Fig. 4 shows the complete stress-strain curves of TiAl(FL) in strain rate 100–800 s^{-1} under tensile impact. The curves are mainly composed of liner elastic section. The specimen break promptly after loading it pass the ultimate stress point. In fact, all of the specimen fractured before they were plastically strained to 0.2%, which makes it impossible to determine the engineering yield stress $\sigma_{0.2}$. From Fig. 4, it is obvious that TiAl(FL) is strain rate sensitive and exhibits high-velocity ductility under tensile impact. This means that the higher the strain rate, the larger is the critical strain in maximum stress of Tial(FL). From the stress-strain curves, the ultimate tensile strength and failure strain can be determined, and their relationship with the strain rate is shown in Fig. 5. It can be observed that UTS and failure strain are perfectly linear with lg $\dot{\varepsilon}$. The average experiment values with different strain rate are listed on Table I.

Fig. 6 shows the tensile fracture surface (SEM) of TiAl(FL) at strain rate 800 s^{-1}. Similar fractographs

TABLE I Material parameters of TiAl(FL) at different strain rate

Strain rate (s^{-1})	E(GPa)	σ_b(GPa)	ε_b(%)	β^I	β^{II}	σ_0^I(GPa)	σ_0^{II}(GPa)
800	95.5	0.4435	0.559	5.394	5.293	0.7296	0.731
300	95.5	0.3725	0.4630	5.833	5.835	0.5983	0.598
100	95.5	0.3085	0.3770	6.473	6.469	0.4804	0.479

I based on Equation 3.4; II based on Equation 3.5.

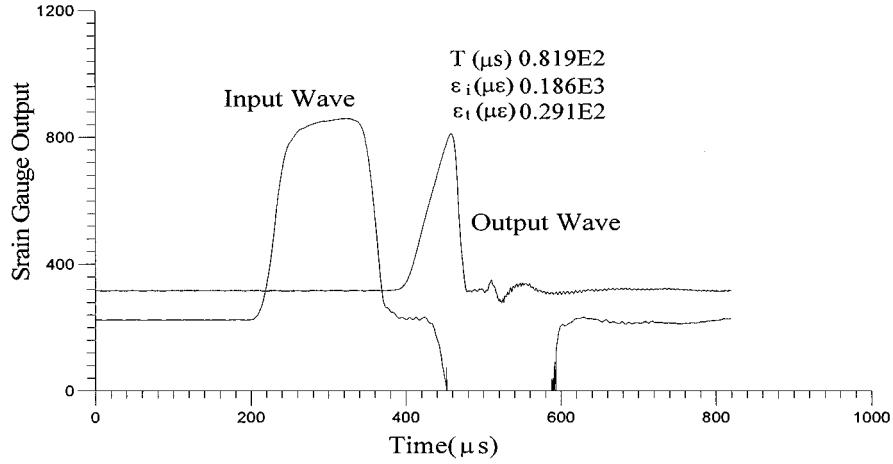

Figure 3 Typical long impulse (specimen broken).

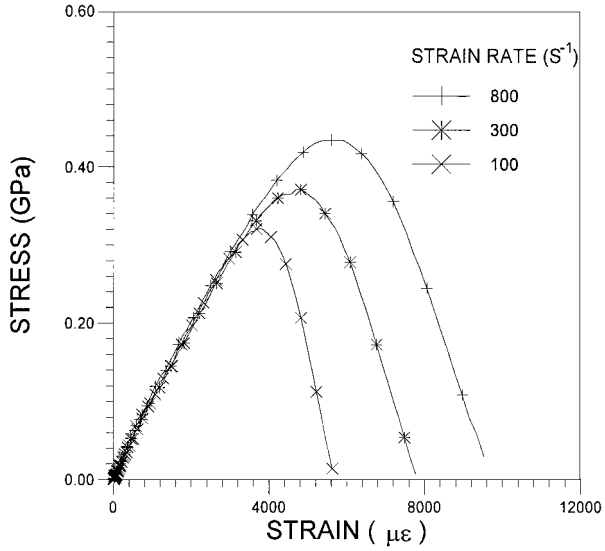

Figure 4 Stress-strain curves of TiAl at different strain rate.

Figure 6 Tensile fracture surface (SEM) of TiAl(FL) at strain rate 800 s^{-1}.

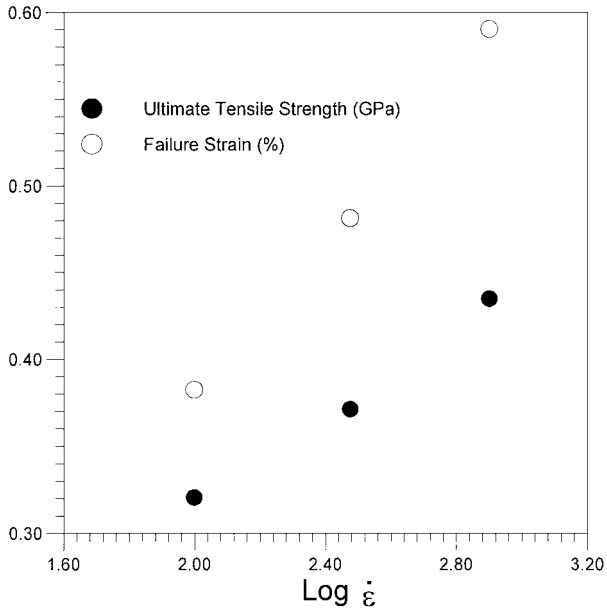

Figure 5 UTS and failure strain of TiAl vs. strain rate.

were observed on the specimen failing at other dynamic strain rate. TiAl(FL) specimen exhibit three characteristic fracture features: delamination (A), set-wise fracture (B), and transamellar fracture (C). The formation of a particular fracture feature appears to depend on the lamellar orientation with respect to the crack path or stress axis. Translamellar fracture or cracking can occure in crack arrest orientation (lamellar boundaries nearly perpendicular to the crack propagation direction), or in the crack divider orientation for which lamellar plates are perpendicular to the crack plane and parallel to the growth direction. Lots of microcrack can be found on the translamellar fracture surface. When the crack propagation direction parallel to the lamellar plates, delamination and step-wise fracture can occur. For delamination and step-wise fracture, fracture surface show relatively even compared with that of translamellar fracture. Few microcrack can be found. The low tensile strength and ductility of large-grained FL microstructures can be explain qualitatively by the characteristic anisotropy of tensile properties of lamellar structures and the resulting strain incompatibility at or across the lamellar grain boundaries.

3. Statistical model of the strain rate dependence of TiAl(FL)

In general, Weibull distribution statistical model is often used to describe the stress-strain relationship of brittle

material because of the disorderness and irregularity of grains. This distribution is based on the theory in which the fracture is controlled by weakest defect of material, the so-called "weakest link theory" [12].

$$H(\sigma) = 1 - \exp\left[-\left(\frac{\sigma}{\sigma_0}\right)^{\beta}\right] \tag{3.1}$$

where $H(\sigma_0)$ is the failure probability of material under an applied dynamic no greater than σ, σ_0 and β denote the scale and shape parameters of Weibull distribution, respectively. If we assume that each grain follows Hook's law up to failure, the macro-relationship between applied dynamic stress σ and strain ε of TiAl(FL) under tensile impact can be obtain as follow.

$$\sigma = E\varepsilon[1 - H(E\varepsilon)] = E\varepsilon \exp\left[-\left(\frac{E\varepsilon}{\sigma_0}\right)^{\beta}\right] \tag{3.2}$$

where E is the initial modulus of TiAl(FL). The maximum stress σ_b and the corresponding failure strain ε_b can be obtained from

$$\frac{d\sigma}{d\varepsilon} = 0 \quad \text{when} \quad \varepsilon = \varepsilon_b$$

i.e.

$$\begin{cases} \sigma_b = E\varepsilon_b \exp(-1/\beta) \\ \varepsilon_b = \dfrac{\sigma_0}{E}\beta^{-1/\beta} \end{cases} \tag{3.3}$$

According to Equations 3.2 and 3.3, two methods are found to determine the Weibull parameters. In the first method, we rewrite the Weibull parameters from Equation (3.3) as

$$\begin{cases} \beta = -\left[\ln\left(\dfrac{\sigma_b}{E\varepsilon_b}\right)\right]^{-1} \\ \sigma_0 = \beta(E\varepsilon_b) \end{cases} \tag{3.4}$$

Thus, σ_0 and β can be calculated from σ_b, ε_b, and E at different strain rate. In the second method, we take double logarithms on both side of Equation 3.2, i.e.

$$\ln\left[-\ln\left(\frac{\sigma}{E\varepsilon}\right)\right] = \beta \ln(E\varepsilon) - \beta \ln(\sigma_0) \tag{3.5}$$

From Equation 3.5, a Weibull plots can be obtained from a test integral stress-strain curves (Fig. 4), so σ_0 and β are determined.

On the basis of Equation 3.5 and experimental results, typical Weibull plots are drawn in Fig. 7. The average values of σ_0 and β derived from the two methods are approximately equal (Table I). Fig. 7 shows that the Weibull plots are linear. The strength of grain therefore obeys the Weibull distribution over the strain-rate range of tests.

The Weibull parameters in Table I are plotted as functions of $\lg \dot{\varepsilon}$ in Fig. 8. It shows that both σ_0 and β are rate-dependent and a linear dependence of σ_0 and β on

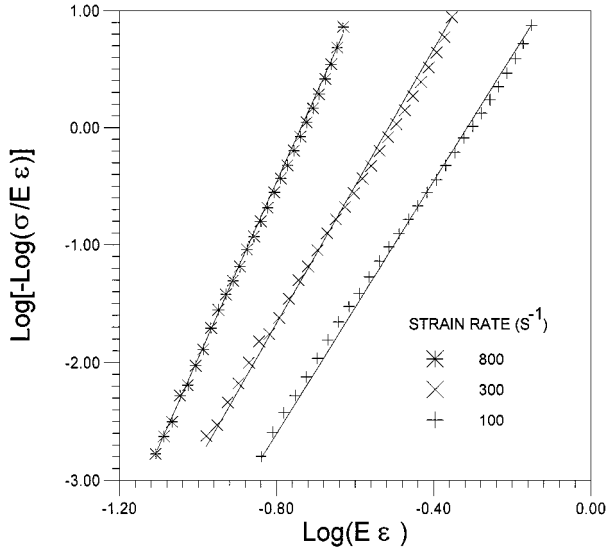

Figure 7 Weibull plots of the strength of TiAl(FL).

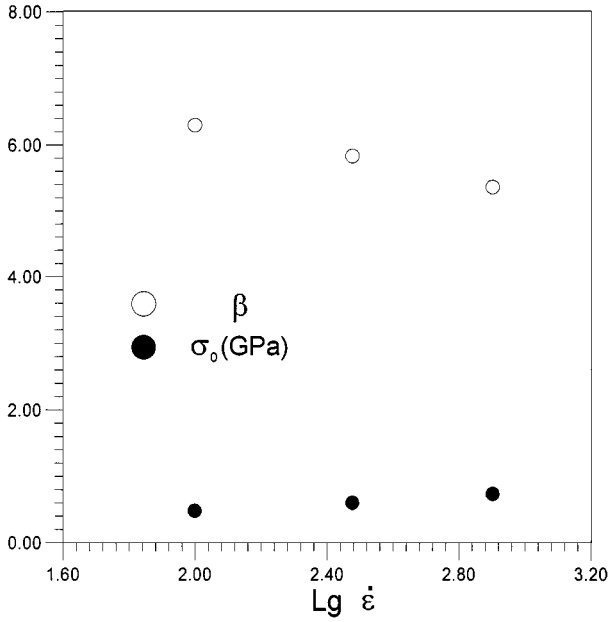

Figure 8 Weibull parameters σ_0 and β vs. $\lg \dot{\varepsilon}$.

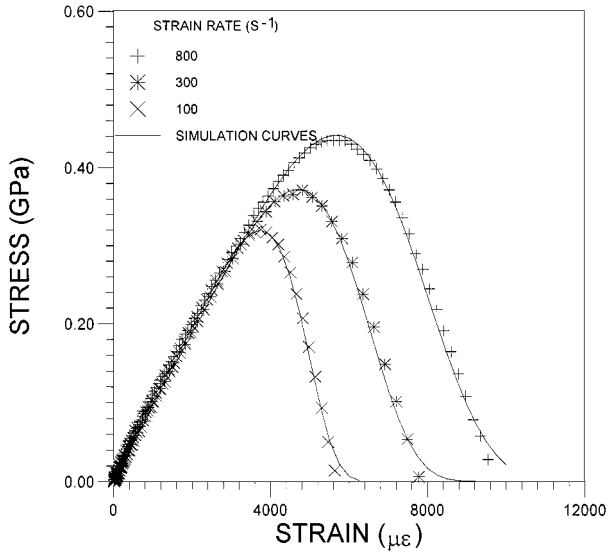

Figure 9 Comparing of simulated stress-strain curves with test data.

lg $\dot{\varepsilon}$ can be found. By using the least square method, we obtain the simulated curves

$$\begin{aligned} \sigma_0 &= -0.279 \log \dot{\varepsilon} + 1.289 \quad \text{(GPa)} \\ \beta &= -4.25 \log \dot{\varepsilon} + 13.85 \end{aligned} \tag{3.6}$$

Substituting the Weibull parameters and modulus obtained from tests into Equation 3.2, the simulated stress-strain curves can be calculated (Fig. 9). The simulated results are very consistent with the experimental data.

4. Conclusion

(1) Experimental studies of TiAl(FL) under tensile impact were performed in the strain rate range from 200 s^{-1} to 800 s^{-1}. Results show that the linear region of stress-strain curves extended to higher strains with increasing strain rate. There was also a corresponding increase in ultimate tensile strength and failure strain with increasing strain rate.

(2) TiAl(FL) specimen exhibit three characteristic fracture features: delamination, set-wise fracture, and transamellar fracture. The formation of a particular fracture feature appears to depend on the lamellar orientation with respect to the crack path or stress axis. Translamellar fracture or cracking can occur in crack arrest orientation (lamellar boundaries nearly perpendicular to the crack propagation direction), or in the crack divider orientation for which lamellar plates are perpendicular to the crack plane and parallel to the growth direction.

(3) Based on Weibull distribution theory, a rate-dependent statistical model was found to describe stress-strain relationship of TiAl(FL) at high strain rate. Simulated results show that the dynamic strength of TiAl(FL) grain obeys the Weibull distribution, both the scale parameter σ_0 and the shape parameter β are linear dependent on lg $\dot{\varepsilon}$, and the simulated stress-strain curves are very consistent with test results.

Acknowledgement

The present work was supported by the National Natural Science Foundation of China.

References

1. Y. W. KIM, *Acta Metall.* **40**(6) (1992) 1121.
2. H. E. DEVE and A. G. EVANS, *Acta Metall. Mater.* **39** (1991) 1177.
3. W. Y. YANG and G. C. WEATHERLY, *J. of Mater. Sci.* **31** (1996) 3707.
4. Z. J. PU, K. H. WU and J. SHI *et al.*, *Mater. Sci. Eng. A* **192/193A** (1995) 347.
5. Y. M. KIM and D. M. DIMIDUK, *JOM* **8** (1991) 40.
6. C. KOEPPE and A. BARTELS *et al.*, *Matel. Trans.* **24A** (1993) 1795.
7. K. S. CHAN and Y. W. KIM, *Metal. Trans. A* **24** (1993) 113.
8. Y. M. KIM, *JOM* **64**(7) (1994) 30.
9. S. A. MALOY and G. T. GRAY. III, *Acta Mater.* **44**(5) 1741.
10. P. S. FOLLANSBEE and G. T. GRAY. III, *Metal. Trans.* **20A** (1989) 863.
11. YUANMING XIA and YUANXIN ZHOU, *ACTA Mechanica Sinica* (English Series) **12**(3) (1996) 243–250.
12. YUANMING XIA, JIANMING YUAN and BAOCHANG YANG, *Composite Science and Technology* **52** (1994) 499–504.

Received 19 January
and accepted 22 July 1999